Decadal Sea Level Variability in the South Pacific in a Global Eddy-Resolving Ocean Model Hindcast

YOSHI N. SASAKI*
Division of Earth and Planetary Sciences, Graduate School of Science, Hokkaido University, Sapporo, Japan

SHOSHIRO MINOBE
Division of Natural History Sciences, Graduate School of Science, Hokkaido University, Sapporo, Japan

NIKLAS SCHNEIDER
Department of Oceanography, and International Pacific Research Center, University of Hawaii at Manoa, Honolulu, Hawaii

TAKASHI KAGIMOTO AND MASAMI NONAKA
Frontier Research Center for Global Change, JAMSTEC, Yokohama, Japan

HIDEHARU SASAKI
Earth Simulator Center, JAMSTEC, Yokohama, Japan

(Manuscript received 25 September 2007, in final form 4 December 2007)

ABSTRACT

Sea level variability and related oceanic changes in the South Pacific from 1970 to 2003 are investigated using a hindcast simulation of an eddy-resolving ocean general circulation model (OGCM) for the Earth Simulator (OFES), along with sea level data from tide gauges since 1970 and a satellite altimeter since 1992. The first empirical orthogonal function mode of sea level anomalies (SLAs) of OFES exhibits broad positive SLAs over the central and western South Pacific. The corresponding principal component indicates roughly stable high, low, and high SLAs, separated by a rapid sea level fall in the late 1970s and sea level rise in the late 1990s, consistent with tide gauge and satellite observations. These decadal changes are accompanied by circulation changes of the subtropical gyre at 1000-m depth, and changes of upper-ocean zonal current and eddy activity around the Tasman Front. In general agreement with previous related studies, it is found that sea level variations in the Tasman Sea can be explained by propagation of long baroclinic Rossby waves forced by wind stress curl anomalies, if the impact of New Zealand is taken into account. The corresponding atmospheric variations are associated with decadal variability of El Niño–Southern Oscillation (ENSO). Thus, decadal sea level variability in the western and central South Pacific in the past three and half decades and decadal ENSO variability are likely to be connected. The sea level rise in the 1990s, which attracted much attention in relation to the global warming, is likely associated with the decadal cooling in the tropical Pacific.

1. Introduction

Long-term sea level variability, in particular, sea level rise, has attracted much attention recently because of its association with global warming (e.g., Church et al. 2001). Cazenave and Nerem (2004), using satellite altimetry data, showed that a trend of sea level rise in the central and western South Pacific (+5–10 mm yr^{-1}) is one of the strongest trends in the world during the period from 1993 to 2003. This prominent sea level trend has been examined by many studies using altimeter data and in situ observations (e.g., Sutton et al. 2005; Qiu and Chen 2006; Bowen et al. 2006; Roemmich et al. 2007). Qiu and Chen (2006) showed that baroclinic Rossby waves forced by wind stress curl anomalies play an important role in the sea level trend.

* Current affiliation: International Pacific Research Center, University of Hawaii at Manoa, Honolulu, Hawaii.

Corresponding author address: Yoshi N. Sasaki, International Pacific Research Center, Post 401, 1680 East-West Road, University of Hawaii at Manoa, Honolulu, HI 96822.
E-mail: sasakiyo@hawaii.edu

DOI: 10.1175/2007JPO3915.1

Roemmich et al. (2007) suggested that the sea level trend is related to a trend of the Antarctic Oscillation (AAO), the leading atmospheric mode in the Southern Hemisphere (Thompson et al. 2000; Mo 2000). This has a substantial implication for future sea level variability in the South Pacific, because the AAO trend may be related to the global warming (e.g., Fyfe et al. 1999; Cai et al. 2003; Meehl et al. 2007).

Sea level variability with a high spatial resolution and global coverage also provides us with precious information on dynamic variations of the gyre circulation, western boundary current, and eddy activity (e.g., Häkkinen and Rhines 2004; Qiu and Chen 2004; Isoguchi and Kawamura 2006; Roemmich et al. 2007). For the South Pacific, Roemmich et al. (2007) reported from in situ and satellite observations that the above-mentioned sea level trend is associated with the spinup of the subtropical gyre at intermediate depths.

However, because the satellite data are available only for the recent one and half decades, it is quite difficult to confidently identify a statistical relation between the decadal trends in sea level and the AAO. It is desirable to extend the sea level record before the satellite era as much as possible. A longer record would increase the confidence in the relationship of decadal sea level variability to the AAO, and in the roles of Rossby waves and gyre adjustments in the decadal trends in sea level. Furthermore, a longer record will determine if the recent sea level trend is part of a long-term secular trend, or if it is the latest example of fluctuations on decadal time scales.

Here, we use three complementary sea level anomaly (SLA) datasets derived from tide gauge, satellite altimeter, and ocean general circulation model (OGCM) output to investigate the long-term variation and dynamics of the South Pacific sea level. Tide gauge observations are available for several decades in the South Pacific (Goring and Bell 1999; Hannah 2004), but their locations are limited to coastal areas. Satellite data have a high spatial coverage, but the temporal availability of the satellite data alone is too short for the present purpose, as mentioned above. Sea level of an extended simulation of an OGCM has high spatial coverage and a longer record than the satellite data, but the realism of the simulation has to be critically examined. Because of these intrinsic problems of the respective datasets, one cannot confidently estimate the decadal sea level changes from only one of three datasets. However, the complementary use of the three datasets, taking account of the specific advantages and disadvantages of each, is expected to provide the most useful information on basin-scale sea level variability on decadal time scales. We verify the spatial pattern and recent time evolution of simulated sea level by comparison with altimeter data, and confirm the long-term veracity of the model with tide gauge observations. Furthermore, for the mechanism of sea level variability, it is known that important roles of long Rossby waves in the South Pacific during the satellite era can be well represented by a linear long Rossby wave model (Qiu and Chen 2006). Thus, we examine whether or not a long Rossby wave model can explain the major sea level variability.

The rest of the present paper is organized as follows: In section 2, models and observational data are explained. The results are described in section 3, with subsections of dominant sea level variability simulated by an OGCM, its relation to ocean circulation changes, comparisons between the sea level variations in an OGCM and a long Rossby wave model, and the relation between the sea level variations and atmospheric fluctuations. A summary and discussion are presented in section 4.

2. Models and data

a. OFES

To reproduce climatological current structures in the South Pacific requires a high-resolution OGCM (e.g., Tilburg et al. 2001). We used output from a 50-yr ocean hindcast of an eddy-resolving OGCM for the Earth Simulator (OFES; Masumoto et al. 2004). The model is based on the National Oceanic and Atmosphere Administration (NOAA)/Geophysical Fluid Dynamics Laboratory (GFDL) third Modular Ocean Model (MOM3; Pacanowski and Griffies 1999) and is described in detail in Sasaki et al. (2004; 2007). The model solves three-dimensional primitive equations in spherical coordinates under the Boussinesq and hydrostatic approximations. The model domain is nearly global and extends from 75°S to 75°N, with a horizontal resolution of 1/10°; there are 54 levels in the vertical cover the ocean from the surface to realistic bottom topography. The model was spun up for 50 yr from a state of rest and climatological temperature and salinity fields of the *World Ocean Atlas 1998* (hereafter *WOA98*; Boyer et al. 1998a,b,c) were used. Although this spinup integration may be not sufficient to reach a steady-state circulation of the abyssal ocean, the effect of the abyssal ocean drift on sea level variations is small and can be ignored. Following the spinup, OFES is forced from 1950 to 2003 with daily surface wind stress, heat flux, and salinity flux based on the National Centers for Environmental Prediction–National Center for Atmo-

spheric Research (NCEP–NCAR) reanalysis data (Kalnay et al. 1996). Surface heat flux is calculated with the bulk formula of Rosati and Miyakoda (1988) from atmospheric variables of the NCEP–NCAR reanalysis data. In addition, sea surface salinity is restored to its monthly climatology of *WOA98* with a time scale of 6 days. At the near-northern and southern artificial boundaries (72°–75°N, S), the temperature and salinity are restored to the monthly mean climatologies of *WOA98* at all depths. The OFES hindcast has already been used to study decadal variability in the North Pacific, and Nonaka et al. (2006) and Taguchi et al. (2007) reported that the hindcast simulation reproduces the decadal variability well. The reliability of the forcing data of the earlier period may be questionable because of insufficient observations used for the NCEP–NCAR reanalysis in the Southern Hemisphere (e.g., Hines et al. 2000). Marshall and Harangozo (2000) showed that mean sea level pressures (SLPs) in the NCEP–NCAR reanalysis over the midlatitude South Pacific are reliable since the early 1970s. Hence, we analyze OFES outputs from 1970 to 2003. To attain a manageable dataset, we reduced the outputs to 1/2° horizontal resolution by subsampling every fifth grid point both in the zonal and meridional directions. Note that the results in the present study do not depend on this subsampling. Monthly anomaly fields are calculated as the difference from the model's monthly climatologies.

Globally averaged SLAs are zero in OFES. That is, OFES does not include sea level changes resulting from the melting of continental ice and does not simulate globally averaged sea level rise resulting from the thermal expansion of seawater. Thus, OFES represents sea level variability caused by wind and regional heat forcings. However, because over the central and western South Pacific these localized SLAs are much larger than the global trend of sea level (Cazenave and Nerem 2004), we expect that SLAs of OFES are sufficient for our purpose. As will be shown in section 3a, OFES reproduces the spatial and temporal structures of the trendlike sea level variation in the South Pacific reported from the satellite data. In addition, the dominant sea level variability of OFES from 1970 to 2003 represents a spatial rearrangement of ocean waters in and above the thermocline, with an amplitude larger than the rate of globally averaged sea level trend during the twentieth century.

b. A long Rossby wave model

To examine the mechanism of sea level variations, we adopt a reduced-gravity long Rossby wave model that has been employed by many studies to investigate SLAs caused by the baroclinic response to wind stress curl anomalies (e.g., Schneider et al. 2002; Fu and Qiu 2002; Qiu and Chen 2006). Qiu and Chen (2006) showed that wind-driven long Rossby waves can explain overall sea level variations in the South Pacific on interannual to decadal time scales since 1992. We investigate whether wind-driven long Rossby waves can account for the dominant sea level variability of OFES from 1970 to 2003. We include the long Rossby wave emanating from New Zealand into the Tasman Sea in response to the incident Rossby wave into New Zealand from the South Pacific Ocean. This effect was ignored by Qiu and Chen (2006), but, as will be shown later, is important for SLAs in the Tasman Sea where the large sea level trend was observed (e.g., Cazenave and Nerem 2004).

The long Rossby wave model solves the linear vorticity equation with a reduced gravity under a long-wave approximation (e.g., Qiu and Chen 2006),

$$\partial_t \eta - c_R \partial_x \eta = -(g'/\rho_0 g f)\mathrm{curl}\boldsymbol{\tau} - \varepsilon\eta \qquad (1)$$

where η is SLA, c_R is the propagation speed of the long baroclinic Rossby wave, f is the Coriolis parameter, ρ_0 is the reference density, g' is the reduced gravity, $|\mathrm{curl}\boldsymbol{\tau}|$ is the magnitude of the wind stress curl anomaly and ε is the Newtonian damping rate. Integrating Eq. (1) westward from the eastern boundary ($x = x_E$) along the baroclinic long Rossby wave trajectories, we obtain

$$\eta(x, y, t) = \eta\left(x_E, y, t + \frac{x - x_E}{c_R}\right)\exp\left[\frac{\varepsilon(x - x_E)}{c_R}\right] + \frac{g'}{\rho_0 g f c_R}\int_{x_E}^{x} |\mathrm{curl}\boldsymbol{\tau}|\left(x', y, t + \frac{x - x'}{c_R}\right)\exp\left[\frac{\varepsilon(x - x')}{c_R}\right]dx', \qquad (2)$$

where x and y are zonal and meridional coordinates, respectively. Wind stress curl anomalies are calculated from the NCEP–NCAR reanalysis data, which has a T62 Gaussian horizontal grid (roughly 1.90° latitude × 1.875° longitude grid). According to Qiu and Chen (2006), $\varepsilon = (6\ \mathrm{yr})^{-1}$ is used. The propagation speed of the baroclinic long Rossby waves is also the same as that used by Qiu and Chen (2006); that is, the propagation speed derived by Chelton et al. (1998), with a latitude-dependent amplification factor of

$A(y) = 1.0 + 0.025(y - 10°\text{S})$ derived by Qiu and Chen (2006), where y is zero at the equator and positive northward, is adopted. The g' value is 0.027 (Qiu 2003). We ignore contributions of SLAs along the South American coast [i.e., $\eta\ (x_E, y, t) = 0$], because the boundary forcing along the South American coast is discounted by dissipation and has little impact on the interior SLAs in the central and western South Pacific (Vega et al. 2003; Qiu and Chen 2006). Thus, the wind stress integrations term of Eq. (2) gives SLAs of the linear model, except for in the Tasman Sea. SLAs in the Tasman Sea will be discussed in the next paragraph.

To estimate the SLAs in the Tasman Sea, we include the long Rossby wave emanating from New Zealand. Liu et al. (1999) investigated the formation process of an island circulation in the reduced-gravity framework and obtained a theoretical solution for the baroclinic coastal Kelvin waves around islands that radiate long Rossby waves to the west (McCalpin 1995; Fu and Qiu 2002). Following Liu et al. (1999), after inputs of alongshore wind stress and incoming long Rossby waves from east of the island are balanced by the dissipation of short Rossby waves on the eastern coast, the value of the SLA of the coastal Kelvin wave along the coast is given constant values as

$$\eta_K = \frac{1}{y_N - y_S}\left[\int_{y_S}^{y_N} \eta_{\mathrm{RL}}(x_{\mathrm{IE}}, y)\, dy - \frac{f_0}{\beta g}\oint_{\text{island}} \frac{\tau_l}{\rho_0 H}\, dl\right], \tag{3}$$

where η_{RL} is SLA caused by incoming long Rossby waves from east of the island, f_0 is the mean Coriolis parameter of the island, β is the meridional gradient of the Coriolis parameter, x_{IE} is the longitudinal location of the eastern coast of the island, y_N and y_S are the latitudinal locations of the northern and southern tips of the island, respectively, and $H = 250$ m is the first layer thickness around the island. The first term on the right-hand side represents the contribution of incoming Rossby waves from east of the island, and the second term represents the contribution of alongshore wind stress. Liu et al. (1999) showed that the wind stress and incoming long Rossby waves balance with the dissipation of short Rossby waves on the eastern coast within an adjustment time of $1/\delta\beta$, where δ is the width of the Munk boundary layer (Pedlosky 1987). This time scale is about 1 month in their model. In our linear model, we calculate the Kelvin wave amplitude from Eq. (3) along the coast of New Zealand at each time step of 1 month, and we use that value as the eastern boundary conditions in the Tasman Sea. Thus, SLAs of the linear model in the Tasman Sea are given by the following three terms of wind stress integrations: SLAs caused by the local wind stress curl anomalies over the Tasman Sea, SLAs caused by the incoming Rossby waves from east of New Zealand, and SLAs caused by the Ekman convergence along New Zealand. In steady state, the sea level obtained from Eq. (3) is identical to that of the "island rule" (Godfrey 1989), which yields transport estimates that are robust generally within 75% of true transports obtained in numerical experiments (Pedlosky et al. 1997).

c. Observational datasets

To compare the sea level variation of OFES with the observations, we use satellite and tide gauge SLA data. Satellite altimetry data combine observations from Ocean Topography Experiment (TOPEX)/Poseidon, *European Remote Sensing Satellite* (*ERS*)*-1/2*, *Jason-1*, and *Environmental Satellite* (*Envisat*), and are provided by Archiving, Validation, and Interpretation of Satellite Oceanographic data (AVISO) on a 1/3° × 1/3° Mercator grid every 7 days from October 1992 to December 2003 (Ducet et al. 2000). For consistency with OFES data, we interpolate the altimetry data onto a grid with a horizontal resolution of 1/2° and calculate monthly averages. Tide gauge data are taken from the Permanent Service for Mean Sea Level (PSMSL; Woodworth and Player 2003).

We also examine the monthly surface geostrophic velocity anomaly data provided by AVISO, monthly surface wind stress, and 500-hPa geopotential height (Z500) data taken from the NCEP–NCAR reanalysis (Kalnay et al. 1996), and the monthly SST dataset provided from the Met Office as the Hadley Centre Sea Ice and Sea Surface Temperature dataset, version 1 (HadISST1; Rayner et al. 2003).

3. Results

a. Sea level variability

Before investigating sea level variability, we briefly summarize the major features of the mean sea surface height of OFES (white contours in Fig. 1). The center of the subtropical gyre is located east of Australia between 15° and 25°S. The East Australian Current (EAC), which is the western boundary current of the subtropical gyre, flows southward along the eastern coast of Australia and divides into the southward current along the coast of Australia as far as Tasmania and the eastward current along the Tasman Front around 34°S between Australia and New Zealand (Andrews et al. 1980; Ridgway and Dunn 2003). Farther south, OFES shows the steep gradients of sea level associated

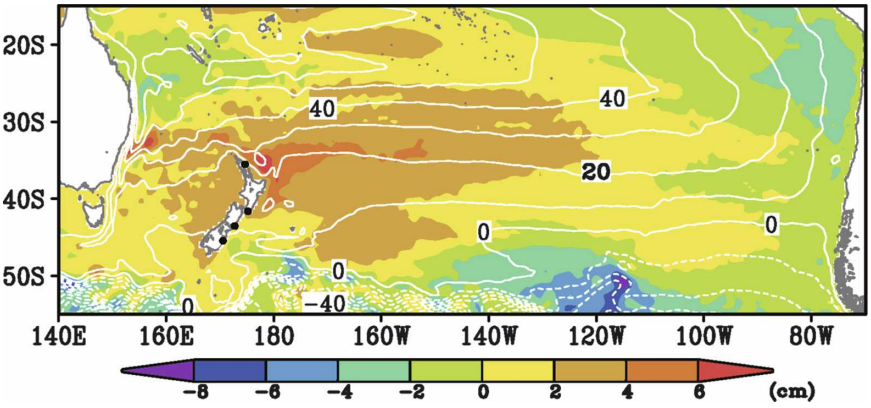

FIG. 1. First EOF of the monthly SLAs of OFES from January 1970 to December 2003. Contours denote the climatology of the sea surface height of OFES, and the contour interval is 10 cm. Closed circles in New Zealand indicate the locations of tide gauge stations, from north to south: Auckland (36°51′S, 174°46′E), Wellington (41°17′S, 174°47′E), Lyttelton (44°24′S, 171°16′E), and Dunedin (45°53′S, 170°30′E).

with the Antarctic Circumpolar Current. These features are consistent with observations (Reid 1986; Ridgway and Dunn 2003).

Figure 1 shows the first EOF mode of the monthly SLAs of OFES (OFES-EOF1) from 1970 to 2003 in the South Pacific (14.5°–59.5°S, 140°E–70°W). This mode explains 10.0% and 22.7% of the total monthly and annual SLA variances, respectively. The reason for the low explained variance of monthly SLAs is that small-scale variations, such as mesoscale eddies, have a lot of energy on intra-annual time scales, but are not efficiently captured by an EOF analysis. Positive SLAs occur from the central South Pacific to the Tasman Sea with large amplitudes around the northeastern coast of New Zealand and the Tasman Front. Negative SLAs are located over the eastern South Pacific, in the Southern Ocean south of 50°S and around the northeastern coast of Australia. This pattern resembles the spatial patterns of the prominent sea level trend reported by previous studies based on the satellite data (e.g., Cazenave and Nerem 2004). Because the second EOF mode of SLAs of OFES explains only 5.7% (13.3%) of the total monthly (annual) SLA variance, and because atmospheric circulation fluctuations related to this mode are not well organized (not shown), we focus our attention on OFES-EOF1 in the present paper.

To compare the sea level fluctuations of OFES-EOF1 to the trend-like sea level variations of the satellite observations, we performed an EOF analysis using monthly SLAs of satellite observations from October 1992 to December 2003. Figure 2 shows the first EOF mode from the satellite data. The overall spatial pattern is similar to that of OFES-EOF1 (Fig. 1), and these two spatial patterns are well correlated ($r = 0.55$).

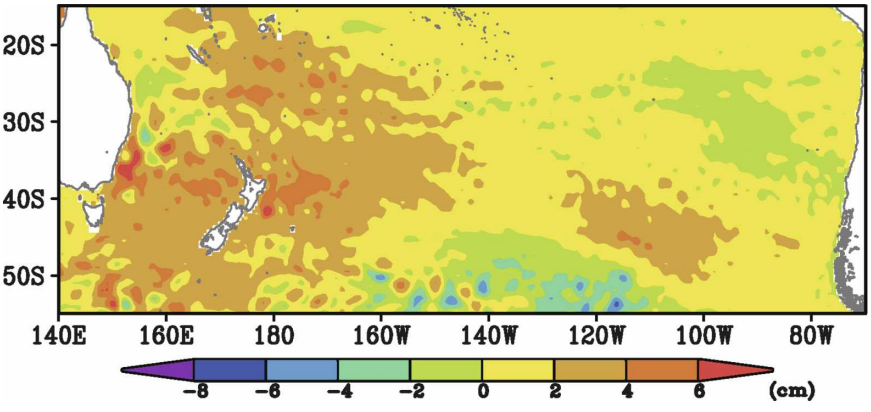

FIG. 2. First EOF of the monthly SLAs of satellite observations from October 1992 to December 2003.

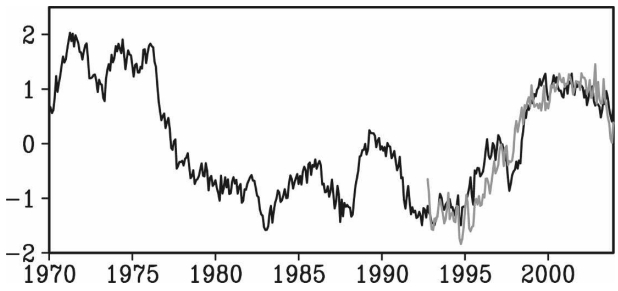

FIG. 3. Normalized PCs of the first EOF modes of the monthly SLAs for OFES from January 1970 to December 2003 (black) and for the satellite from October 1992 to December 2003 (gray) with the corresponding spatial patterns shown Figs. 1 and 2, respectively.

The spatial map of the satellite also shows positive SLAs from the central South Pacific to the Tasman Sea with the large amplitudes around the northeastern coast of New Zealand and the Tasman Front and negative SLAs in the Southern Ocean south of 50°S and around the northeastern coast of Australia. Furthermore, these SLA amplitudes found in both satellite and OFES maps are comparable. Although SLAs of the satellite are generally positive in the eastern South Pacific in contrast to the negative values of OFES-EOF1 there, amplitudes of EOF1 both from the OFES and satellites are small in this region. It seems that eddy-like small-scale SLAs are more prominent in the satellite than in OFES, but this is primarily due to the data length difference between the satellite and OFES. Indeed, the regression map of the OFES SLAs for the same period as that of the satellite data (from October 1992 to December 2003) onto the principal component (PC) of OFES-EOF1 exhibits more prominent eddy-like SLAs than the map of OFES SLAs from 1970 to 2003 (not shown). In addition, the former map is better correlated with the regression map of the satellite shown in Fig. 2 ($r = 0.65$). Hence, OFES successfully simulates the spatial structure of observed dominant variability of sea level in the last decade.

The PCs of the first EOF modes for the satellite and OFES both exhibit trendlike sea level variations after 1992, and these two PCs are highly correlated ($r = 0.94$; see Fig. 3). The two PCs were negative from the beginning of the satellite record, that is, 1992, to the mid-1990s, rapidly increased to the positive values in the late 1990s, and remained positive until the end of the record. Therefore, OFES reproduces the observed trend-like variations of sea level during the last decade well.

The prominent trend after 1992 was not persistent a priori to the satellite era in the PC of OFES-EOF1 (black line in Fig. 3). Instead, the PC for the entire period from 1970 to 2003 appears to be dominated by decadal fluctuations. Starting from a positive phase in the early and mid-1970s, the PC rapidly decreased to a negative phase in the late 1970s. The polarity of the PC generally stayed negative during the period from the early 1980s to the mid-1990s, with near-zero values around 1990. In the late 1990s, as mentioned above, the PC rapidly increased to the positive phase and continued to be positive phase until the end of the data. The maximum sea level differences of OFES-EOF1 between the positive phase (i.e., in the early 1970s and the late 1990s) and the negative phase (i.e., from the early 1980s to mid-1990s) are about 12 cm (Figs. 1 and 3), and thus this amplitude is larger than the amplitudes of the global mean sea level rise during the twentieth century [e.g., +4.5 cm (30 yr)$^{-1}$; Church et al. 2001] and that from 1993 to 2003 [e.g., +2.8 cm (11 yr)$^{-1}$; Cazenave and Nerem 2004]. The steplike phase shift in the late 1970s combined with the persistency of the positive (negative) phase in the early 1970s (from the early 1980s to the mid-1990s) is reminiscent of so-called the climate regime shift (e.g., Minobe 1997) associated with the decadal variability of El Niño–Southern Oscillation (ENSO; e.g., Zhang et al. 1997), the interdecadal Pacific oscillation (Folland et al. 1999; Power et al. 1999), or the Pacific (inter)decadal oscillation (Mantua et al. 1997). It is noteworthy that in the late 1990s oceanic and atmospheric changes occurred over and around the Pacific Ocean with an opposing polarity to the 1970s regime shift (e.g., Minobe 2002; Chavez et al. 2003), consistent with the decadal changes of OFES-EOF1. The relation of OFES-EOF1 to these climate changes will be further discussed in section 3d.

To know whether the sea level changes of OFES-EOF1 before 1992, especially the rapid sea level fall in the late 1970s, are realistic or not, we examine tide gauge SLA data along the New Zealand coast for Auckland, Wellington, Lyttelton, and Dunedin (Hannah 2004), where SLAs are especially large (the locations of the tide gauges are shown in Fig. 1). To remove intra-annual variability, we use the annual averages for those years that have at least 9 months of data. Because OFES-EOF1 shows the large-scale sea level variations, we check whether or not the sea level variations of the tide gauge data represent large-scale sea level variations around New Zealand. For this purpose, we calculate the correlations between all pairs of tide gauge datasets during the time of overlap from 1970 to 2003. All resultant correlations are significant at the 90% confidence level, except for the correlation between Lyttelton and Auckland ($r = 0.04$) and the correlation between Lyttelton and Dunedin ($r = -0.06$). Hence, we excluded the data at Lyttelton. Table 1 shows the

TABLE 1. Correlation coefficients between the annual averages of the PC of OFES-EOF1 and annual averages of sea level from tide gauges at Auckland, Wellington, and Dunedin. The location of each station is shown in Fig. 1. The "global mean trend removed" column indicates that the global mean sea level trend during the twentieth century of +1.5 mm yr^{-1} (Church et al. 2001) is removed from each tide gauge time series. The rightmost column indicates the number of available years of tide gauge observations.

	r		
	Raw	Global mean trend removed	No. of years
Auckland	0.50	0.72	28
Wellington	0.41	0.60	28
Dunedin	0.82	0.85	15

correlations between the annual averages of the PC of OFES-EOF1 and observed SLAs at the three stations. All correlations are positive and significant at the 95% confidence level, consistent with the large-scale positive SLAs around New Zealand (Fig. 1).

The sea level variations at the three stations are not only qualitatively but also quantitatively similar to the sea level variations of the OFES-EOF1 reconstructed around New Zealand. As an example, Fig. 4 shows the annual averages of SLAs at Auckland obtained from the tide gauge and reconstructed from OFES-EOF1. The Auckland data also support a rapid sea level fall in the late 1970s. Therefore, these results suggest that the major features of the temporal changes of OFES-EOF1 are consistent with the observations before the satellite era. The sea level fall in the late 1970s in the northern New Zealand is also reported by Goring and Bell (1999) from tide gauge data.

As mentioned in section 2a, SLAs of OFES do not include the globally averaged sea level trend. If we remove from the observed sea level time series the global mean sea level trend during the twentieth century of +1.5 mm yr^{-1} (Church et al. 2001), the correlations with the annual averages of the PC of OFES-EOF1 increase from those using the raw time series of the tide gauges (the third column to the second in Table 1).

For a further examination of the validity of OFES SLAs in the early period, we compare SST variability corresponding to OFES-EOF1 between observations and OFES. Because both SST anomalies and SLAs are partly caused by surface heat fluxes and the Ekman pumping, and because SLAs contribute to the generation of SST anomalies through horizontal advection, large-scale sea level variability is expected to be tightly related to large-scale SST variability. Therefore, a comparison of observed and OFES SSTs may provide useful information regarding whether or not OFES SLAs are reliable, including their spatial pattern, which cannot be examined using tide gauge data. Figure 5 shows the correlation maps of the SST of HadISST1 and OFES with the PC of OFES-EOF1. The correlations are positive from the central South Pacific to the Tas-

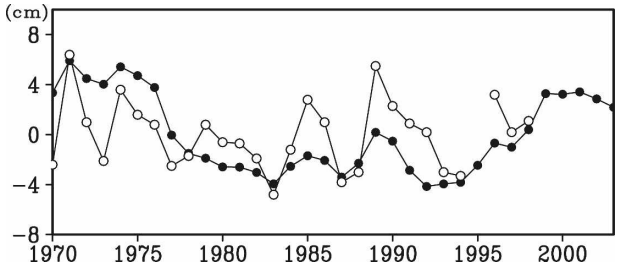

FIG. 4. Reconstructed annual averages of SLAs from OFES-EOF1 at a grid point (35.95°S, 174.55°E) around Auckland (closed circles) and observed annual averages of SLAs from the tide gauge at Auckland (open circles).

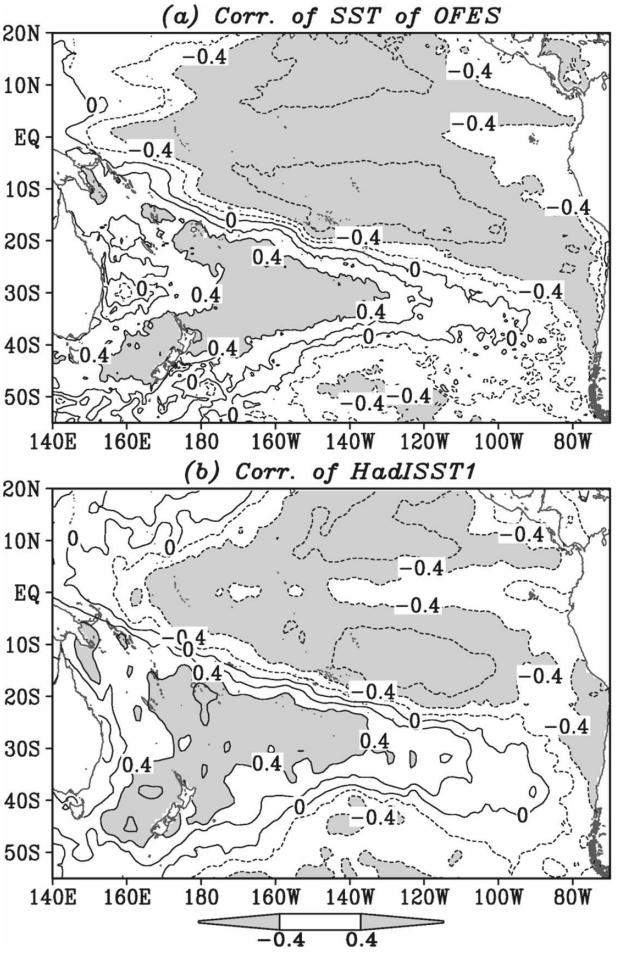

FIG. 5. (a) Correlation coefficients of monthly OFES SST onto the PC of OFES-EOF1, (b) and those of observed SST onto the same time series. The contour interval is 0.2.

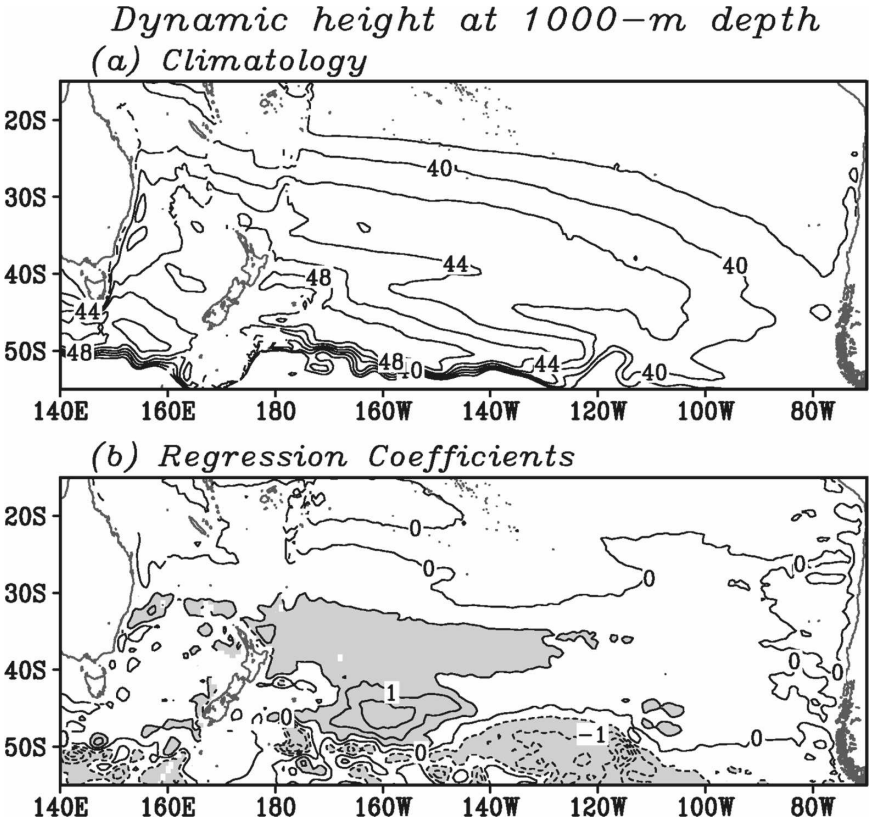

FIG. 6. (a) Climatology of the dynamic height of OFES at 1000-m depth. The contour interval is 2 cm, and contours <38 cm are not drawn. (b) Regression coefficients of the dynamic height of OFES at 1000-m depth from 1970 to 2003 onto the PC of OFES-EOF1; before calculating the regressions, a 9-month running mean filter is applied to the dynamic height data and the PC of OFES-EOF1; the contour interval is 0.5 cm, and shading indicates the regions where the absolute regressions are greater than 0.5 cm.

man Sea, and negative in the northeastern and southeastern South Pacific in both the observations and OFES outputs. We also calculate the SST correlation maps using the HadISST1 and OFES data only before 1992, and these two maps are similar to those shown in Fig. 5 (not shown). Hence, these similarities of the two SST patterns support that OFES outputs are realistic from 1970 to 2003 in the South Pacific. Note also that these SST patterns resemble the pattern associated with decadal ENSO variability (e.g., Garreaud and Battisti 1999), whose relation with OFES-EOF1 will be discussed in section 3d.

b. Relation to ocean circulation changes

The basin-scale spatial structures of SLAs captured by OFES-EOF1 (Fig. 1) suggest that the corresponding sea level variation accompanies changes of the subtropical gyre. Indeed, from their in situ and satellite data Roemmich et al. (2007) showed that the regional sea level rise was associated with the spinup of the subtropical gyre at 1000 m during the late 1990s. To examine whether this association also occurred in the past, we calculated dynamic heights of OFES at 1000-m depth,

$$h = \frac{1}{\rho_0} \int_{-z_0}^{-1000} [\rho_0 - \rho(z)]\, dz, \tag{4}$$

where ρ is the density, ρ_0 is the reference density, z is the depth, and z_0 is the reference depth at 1800-m depth, consistent with Roemmich et al. (2007).

OFES simulates the major features of the mean ocean circulation at 1000-m depth (Fig. 6a). The center of the subtropical gyre is located east of New Zealand between 40° and 50°S, and the southward western boundary current is located along the coast of Australia, and reaches as far as Tasmania. These features are consistent with those of the observations (Reid 1986; Ridgway and Dunn 2003).

Let us now examine the circulation changes corresponding to OFES-EOF1. Because we are interested in

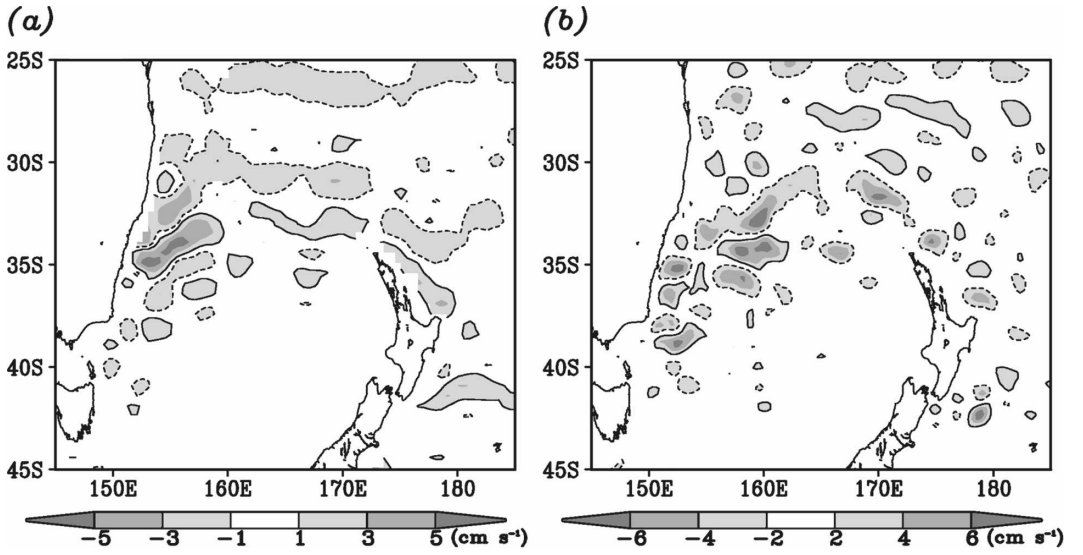

FIG. 7. Regression coefficients with respect to the PC of OFES-EOF1 (a) for the zonal velocity of OFES at 200-m depth from 1970 to 2003, and (b) for the satellite-derived zonal geostrophic velocity from October 1992 to December 2003. Before calculating the regressions, a 9-month running mean filter is applied to the velocity data and the PC of OFES-EOF1. Solid (dashed) contours denote positive (negative) regressions, and only contours of (a) ±1 and (b) ±2 cm s^{-1} are drawn.

interannual to decadal variability, a 9-month running mean filter is applied to the data. Hereafter, we use the term "low-pass filter" to refer to the filter, unless otherwise stated. Figure 6b shows the regression coefficients of the dynamic height onto the PC of OFES-EOF1. The positive anomalies occur east of New Zealand between 30° and 50°S and between Australia and New Zealand at 34°S, while the negative anomalies occur in the Southern Ocean south of 50°S. This pattern of the dynamic height resembles that of the OFES-EOF1 for SLAs (Fig. 1). In addition, the positive dynamic height anomalies increase the slope of the dynamic height (Fig. 6) and suggest a spinup of the subtropical gyre at 1000-m depth, consistent with the observed changes in the 1990s (Roemmich et al. 2007). Hence, the association between the sea level variation captured by OFES-EOF1 and the strength changes of the subtropical gyre at 1000-m depth continuously holds during the period from 1970 to 2003. Note that this result does not necessarily imply a spinup of the subtropical gyre at shallower levels, because the gyre center shifts with height toward the east of Australia (Fig. 1; e.g., Reid 1986), and is collocated with action centers of neither dynamic heights nor SLAs.

In addition to the relation with the large-scale gyre circulation, an interesting question is whether the basin-scale sea level variations of OFES-EOF1 accompany small-scale variations of western boundary currents. The spatial pattern of OFES-EOF1 exhibits not only the large-scale SLAs but also the small-scale SLAs, such as around the northeastern coast of New Zealand and in the Tasman Sea (Fig. 1). We focus on the EAC regions where the small-scale SLAs occur (Fig. 1) and highly energetic currents are observed (e.g., Ridgway and Dunn 2003). For a comparison of the velocity changes between the satellite data and OFES outputs, we use the velocity of OFES at 200-m depth to avoid the effects of near-surface Ekman velocity components, which are not included in the geostrophic velocity estimated from the satellite altimeter. Only zonal velocity changes associated with OFES-EOF1 are discussed, because the zonal velocity changes are more organized and have larger amplitudes than the meridional velocity changes in these regions. The zonal velocity anomalies around the separation point of the EAC are large in both the satellite data and OFES outputs (Fig. 7). In addition, the negative zonal velocity anomalies around the separation point of EAC extend along the northern part of the Tasman Front (30°–33.5°S) in both the observations and OFES, although narrower positive velocity anomalies located to the south of these negative velocity anomalies in OFES are not seen in the observations. The negative zonal velocity anomalies along the northern part of the Tasman Front are consistent with the positive SLAs in the Tasman Sea (Fig. 1). In OFES, negative bandlike anomalies along 25°–27°S and positive bandlike anomalies east of New Zealand around 40°–42°S are clearly seen, although in observations, the zonal velocity anomalies around these regions exhibit eddy-like anomalies rather than band-

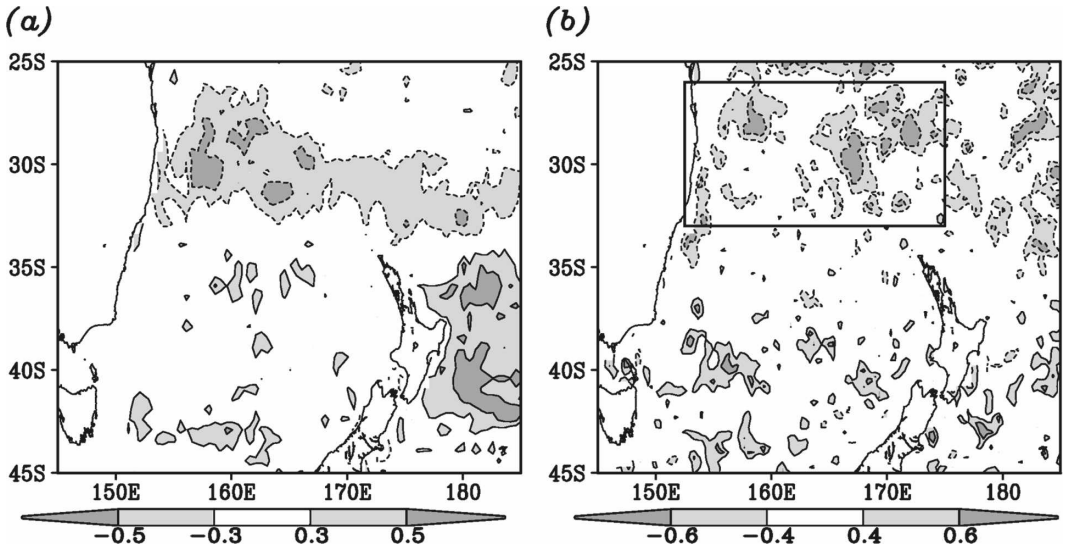

FIG. 8. Correlation coefficients with respect to the PC of OFES-EOF1 (a) for the EKE of OFES at the surface from 1970 to 2003, and (b) for the satellite-derived EKE from October 1992 to December 2003. Before calculating the correlations, a 9-month running mean filter is applied to the velocity data and the PC of OFES-EOF1. The contour interval is 0.2, and the absolute values of correlations below 0.3 and 0.4 are not drawn in the left and right panels, respectively. Solid (dashed) contours denote positive (negative) correlations. The box in the right panel is the region (26°–33°S, 152.5°–175°E) where the area-averaged EKE anomalies in Fig. 9 are calculated.

like anomalies. This difference may be due to the different data length between the two data sets. Indeed, the regression map of the zonal velocity from October 1992 to December 2003 onto the PC of OFES-EOF1 exhibits eddy-like anomalies there (not shown). Therefore, these results suggest that the basin-scale sea level fluctuations accompany the narrow current changes along the Tasman Front on decadal time scales.

These current changes along the Tasman Front may be accompanied by eddy activity changes around the front where eddy activity is large (e.g., Qiu and Chen 2004). To examine eddy activity changes associated with OFES-EOF1, we calculate the correlations between the low-pass-filtered PC of OFES-EOF1 and the low-pass-filtered surface eddy kinetic energy (EKE), defined as $(u^2 + v^2)/2$, where u and v indicate surface zonal and meridional velocity anomalies, respectively. The negative correlations in the northern part of the Tasman Front occur in both the observations and OFES outputs (Fig. 8). Although the extent of the surface EKE anomalies of the satellite is smaller than that of OFES, the temporal EKE variations of OFES averaged in the northern part of the Tasman Front are quite similar to those of the satellite data ($r = 0.93$; see the black dashed line and gray solid line in Fig. 9). The surface EKE anomalies of OFES averaged in this region are also well correlated with the PC of OFES-EOF1 ($r = -0.67$; see the black solid line and black dashed line in Fig. 9), confirming that surface EKEs in this regions are related to basin-scale SLA changes. These negative correlations in the northern part of the Tasman Front seem to correspond to the negative zonal velocity changes along the Tasman Front (Fig. 7). Because the main mechanism generating high eddy variability along the Tasman Front is the movement of the meander and eddy shedding caused by instability processes of strong currents (Andrews et al. 1980; Tilburg et al. 2001), a reduction of the eddy activities in the northern part of the Tasman Front is consistent with the weakening of the flow along the Tasman Front (Fig. 7). Hence, these results suggest that the large-scale sea level variations are related to the small-scale eddy activities through the changes of the ocean jets, such as those found along the Tasman Front. Although the recent studies by Bowen et al. (2005) and Mata et al. (2006) observed mesoscale SLAs propagating southward along the eastern coast of Australia, Fig. 8 shows that OFES-EOF1 does not accompany the eddy activity changes there. The major discrepancy in EKE between OFES and satellite data is found just east of New Zealand's North Island (Fig. 8). This is due to the unrealistic intensification of the quasi-stationary, anticyclonic East Cape Eddy (Ridgway and Dunn 2003) in OFES.

c. A long Rossby wave model

As described in the previous sections, the sea level variations captured by OFES-EOF1 are reasonable

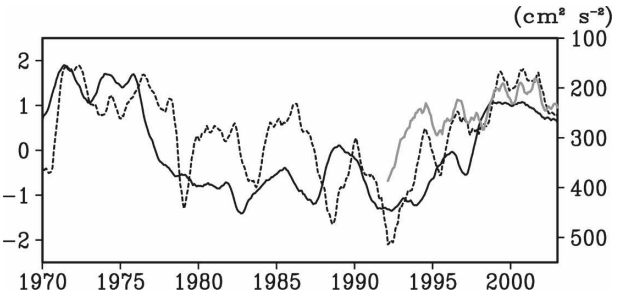

FIG. 9. Surface EKE anomalies of OFES (black dashed line, right axis) and satellite-derived EKE anomalies (gray solid line, right axis) averaged over the northern part of the Tasman Front (26°–33°S, 152.5°–175°E shown by the box in Fig. 8) along with the PC of OFES-EOF1 (black solid line, left axis). A 9-month running mean filter is applied to the all time series. Note that the direction of the right axis is reversed.

from 1970 to 2003. In addition, these sea level variations are accompanied by the changes of the subtropical gyre and the changes of the velocity and eddy activity around the Tasman Front. What is the mechanism of the sea level variations of OFES-EOF1? In this section, we examine whether the sea level variations of OFES-EOF1 can be explained by wind-driven long Rossby waves using the linear model described in section 2b.

Figure 10 shows the regression map of the SLAs of the linear model onto the PC of OFES-EOF1. The overall spatial structures and amplitudes show a good agreement with those of the OFES (Fig. 1). The linear model reproduces positive SLAs from the central South Pacific to the Tasman Sea and negative SLAs in the Southern Ocean south of 50°S and along the northeastern coast of Australia. An EOF analysis of monthly SLAs of the linear model from 1970 to 2003 yields a spatial pattern that is quite similar to the map shown in Fig. 10. Hence, the overall SLAs of OFES-EOF1 can be explained by long baroclinic Rossby waves caused by wind variations. However, the large-amplitude and small-scale SLAs of OFES-EOF1 around the northeastern coast of the New Zealand and the Tasman Front are not reproduced by the linear model. Other mechanisms, such as baroclinic Rossby waves generated by a barotropic mode over a ridge (e.g., Barnier 1988), may be important in these regions where the bathymetry plays a significant role in the flow fields (Andrews et al. 1980; Tilburg et al. 2001; Ridgway and Dunn 2003), but further investigation of this issue is beyond the scope of this paper.

It is important to know whether baroclinic Rossby waves explain sea level variations and the large observed trend (Fig. 1; e.g., Cazenave and Nerem 2004) in the Tasman Sea that are likely to be related to the weakening of the flow along the Tasman Front (Fig. 7). Figure 11 shows SLAs averaged in the Tasman Sea (38.5°–45°S, 150°–170°E) of OFES and the linear model. The linear model successfully reproduces the sea level variations of OFES ($r = 0.84$). This indicates that sea level variations in the Tasman Sea can be explained by wind-driven long Rossby waves if the impact of the island of New Zealand is taken into account (Liu et al. 1999).

As mentioned in section 2b, SLAs of the linear model in the Tasman Sea can be separated into the three components. The first component is due to the local wind stress curl anomalies over the Tasman Sea, the second component is due to the incoming Rossby waves from east of New Zealand, and the third component is due to the Ekman convergence along New Zealand. Because these components have vastly different predictabilities, we determine their relative contributions by the rate of variance reduction and the correlation coefficient. The rate of variance reduction is

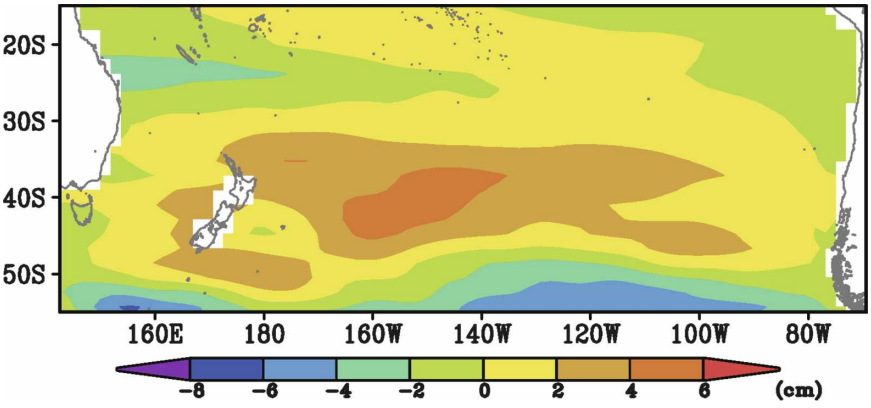

FIG. 10. Regression coefficients of the monthly SLAs of the linear model from 1970 to 2003 onto the PC of OFES-EOF1.

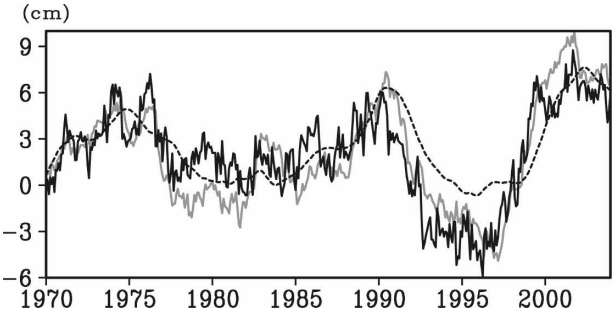

FIG. 11. Monthly SLAs averaged over the Tasman Sea (38.5°–45°S, 150°–170°E) of OFES (black solid line), those of the linear model (gray solid line), and those contributed by the incoming Rossby wave from east of New Zealand in the linear model (black dashed line).

defined as one minus a rate, which is the variance of the area-averaged time series difference between the SLAs of one component of the linear model and OFES SLAs, relative to the variance of area-averaged OFES SLAs, with the Tasman Sea as the average area. The variance reduction from the incoming Rossby waves (52.6%) is larger than that from the Ekman convergence along New Zealand (33.7%) and that from the local wind stress curl over the Tasman Sea (2.4%). Also, the largest correlation between the SLAs of each component of the linear model averaged in the Tasman Sea and SLAs of OFES averaged in the same region is found for the incoming Rossby waves ($r = 0.73$). Hence, the incoming Rossby waves from east of New Zealand are the most important component for sea level variations in the Tasman Sea (black dashed line in Fig. 11). This result implies that the major part of sea level variability in the Tasman Sea is predictable from the sea level to the east of New Zealand. Recently, Sutton et al. (2005) suggested that the sea level rise in the Tasman Sea in the late 1990s cannot be explained by the local Ekman pumping in the Tasman Sea. This sea level rise is mainly attributable to the incoming Rossby wave from east of New Zealand (Fig. 11).

d. Relation to atmospheric circulation changes

The results of the previous section indicate that the excitation of long Rossby waves by wind stress curl anomalies can account for the overall SLAs of OFES-EOF1. To know the associated atmospheric forcing, in Fig. 12 we show the lag regression coefficients of the low-pass-filtered wind stress curl anomalies onto the low-pass-filtered PC of OFES-EOF1. All of the panels in Fig. 12 exhibit the broad positive wind stress curl

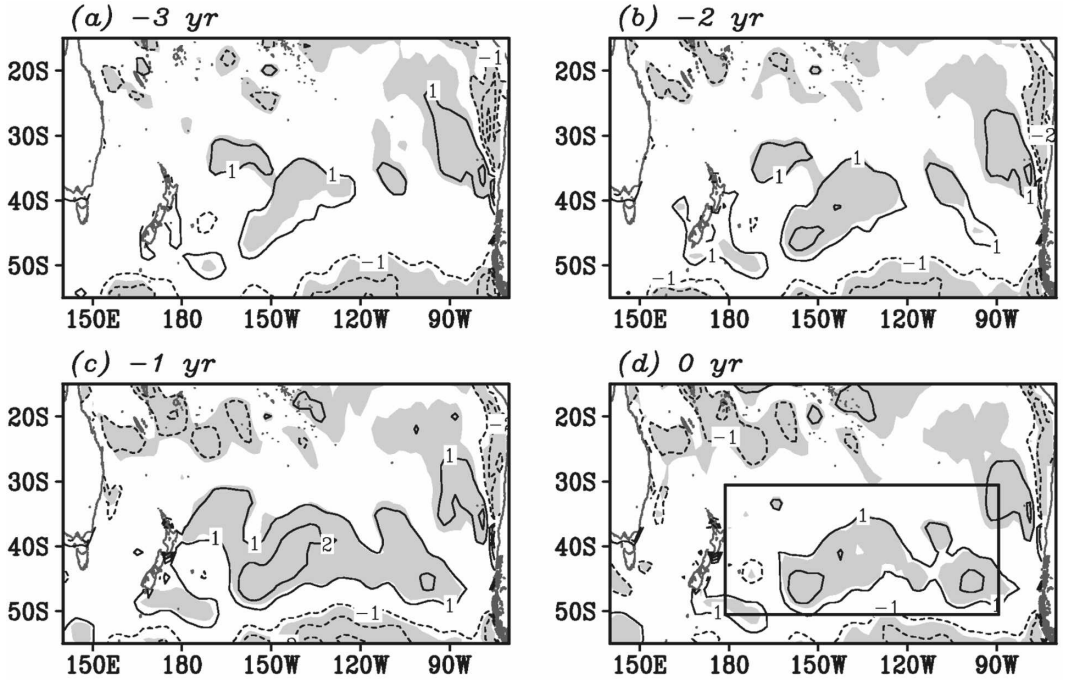

FIG. 12. Lag regression coefficients of the low-pass-filtered monthly wind stress curl from 1970 to 2003 onto the low-pass-filtered PC of OFES-EOF1 for the lag years of (a) −3, (b) −2, (c) −1, and (d) 0, where negative lag means that the PC lags wind stress curl anomalies. The contour interval is 10^{-8} N m^{-2}, and the 0 contour is not drawn. Shading indicates the regions where the absolute correlations are greater than 0.3. The box in (d) indicates the region (30°–50°S, 90°W–180°) where the area-averaged wind stress curl anomalies shown in Fig. 13 are calculated.

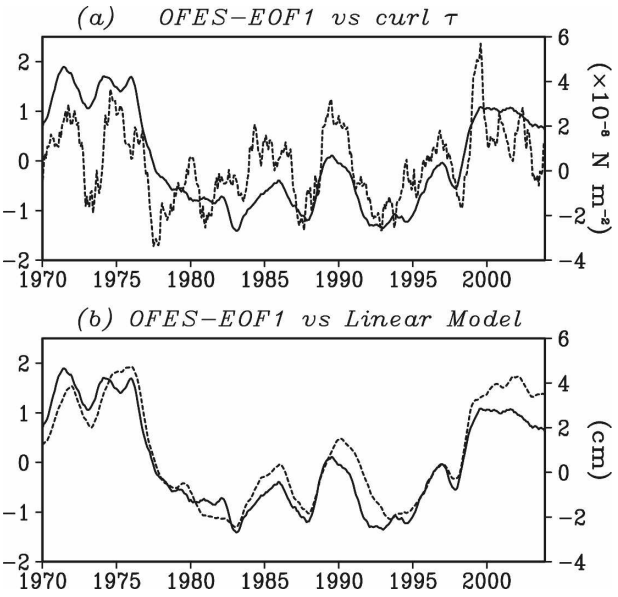

FIG. 13. (a) The low-pass-filtered PC of OFES-EOF1 (solid line, left axis) and the low-pass-filtered wind stress curl anomalies averaged over 30°–50°S, 90°W–180° (dashed line, right axis). The time series of wind stress curl anomalies are shifted backward by 10 months. (b) The low-pass-filtered PC of OFES-EOF1 (solid line, left axis) and the low-pass-filtered SLAs of the linear model averaged over 30°–50°S, 90°W–180° (dashed line, right axis).

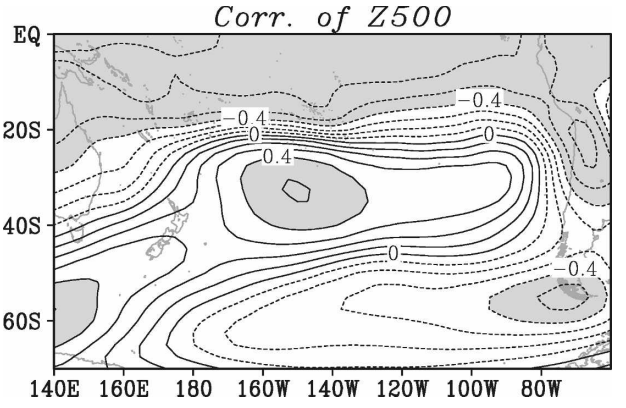

FIG. 14. Correlation coefficients of the low-pass-filtered monthly Z500 anomalies from 1970 to 2003 onto the low-pass-filtered PC of OFES-EOF1, where the PC lags the monthly Z500 anomalies by 10 months. The contour interval is 0.2, and shading indicates the regions the absolute correlations are greater than 0.4.

anomalies over the central South Pacific and the negative anomalies over the northwestern South Pacific and along the coast of South America for the positive phase of OFES-EOF1. When the wind stress curl leads the PC of OFES-EOF1 by 0–1 yr, the positive anomalies over the central South Pacific are especially large. Because positive wind stress curl anomalies yield Ekman convergence there, and because the first baroclinic Rossby wave propagates westward with speeds of about 5°–13° yr^{-1} or less at 30°–50°S (e.g., Maharaj et al. 2005; Qiu and Chen 2006), these positive wind stress curl anomalies are consistent with the lagged positive SLAs in the central and western South Pacific (Fig. 1).

Consistently, the time series of the low-pass-filtered wind stress curl anomalies averaged over the central South Pacific (30°–50°S, 90°W–180°) are highly correlated with the low-pass-filtered PC of OFES-EOF1 ($r = 0.61$), when the former leads the latter by 10 months (Fig. 13a). The wind stress curl anomalies have relatively stronger interannual variability compared with their decadal variability than sea level variability of the linear model forced by wind stress curl anomalies. The low-pass-filtered time series of SLAs of the linear model averaged in the central South Pacific exhibit dominant decadal variability over interannual variability and are strikingly similar to the low-pass-filtered PC of OFES-EOF1 ($r = 0.94$; see Fig. 13b). This is because SLAs result from the time integration of wind stress curl anomalies along baroclinic Rossby wave trajectories [Eq. (2)], and the time integration acts as a temporal low-pass filter.

How is large-scale atmospheric circulation variability related to OFES-EOF1? To this end, we calculate the correlation map between the low-pass-filtered PC of OFES-EOF1 and the low-pass-filtered Z500 10 months earlier to account for the lag associated with the linear Rossby wave dynamics (Fig. 14). The correlation pattern exhibits broad positive correlations between 20° and 45°S over the central South Pacific and negative correlations over the Southern Ocean south of 50°S, and this Z500 pattern resembles the Pacific–South American (PSA) pattern (Karoly 1989), the major Southern Hemisphere atmospheric teleconnection pattern related to ENSO (Karoly 1989; Garreaud and Battisti 1999; Mo 2000). The broad positive correlations of Z500 over the central South Pacific are consistent with the positive wind stress curl anomalies there (Fig. 12). Although the PSA pattern involves both interannual and decadal variability, the aforementioned integral effect associated with oceanic Rossby waves will make ocean responses more sensitive to decadal forcings of the PSA pattern. Therefore, it is suggested that the sea level variations of OFES-EOF1 are related to the atmospheric fluctuations associated with the decadal ENSO. This suggestion agrees with the above-mentioned result that the correlation maps of SST shown in Fig. 5 resemble the pattern corresponding to the decadal ENSO.

For a further investigation on the relation between OFES-EOF1 and decadal ENSO, we define an index of decadal ENSO. To obtain the index, we perform an

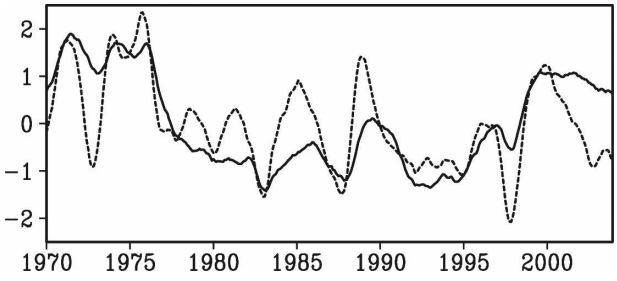

FIG. 15. The low-pass-filtered PC of OFES-EOF1 (solid line) and the low-pass-filtered index of the decadal ENSO (dashed line). The decadal ENSO index is obtained by projecting the spatial pattern of the first EOF mode of the 7-yr low-pass-filtered SST in the equatorial Pacific (20°S–20°N, 120°E–70°W) onto the unfiltered SST in the same region. The sign of the decadal ENSO index is reversed (warmer SSTs toward the bottom of the figure).

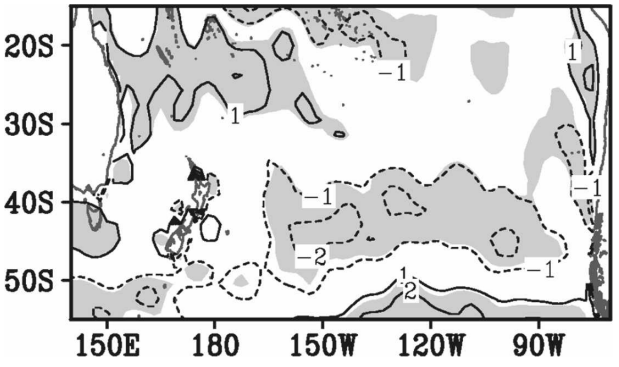

FIG. 16. Regression coefficients of a low-pass-filtered monthly wind stress curl from 1970 to 2003 onto the low-pass-filtered index of the decadal ENSO (Fig. 15). The contour interval is 10^{-8} N m^{-2}, and the 0 contour is not drawn. Shading indicates the regions where the absolute correlations are greater than 0.3.

EOF analysis of the 7-yr low-pass-filtered SST of HadISST1 in the equatorial Pacific (20°S–20°N, 120°E–70°W) from 1970 to 2003, and we project the spatial pattern of this first EOF mode onto the unfiltered SST anomalies in the same region. The correlation coefficient between the low-pass-filtered index of the decadal ENSO and the low-pass-filtered PC of OFES-EOF1 is −0.68 (notice that the decadal ENSO index is sign reversed in Fig. 15). This negative value means that when the decadal ENSO is positive in phase, corresponding SLAs in the central and western South Pacific are negative. Therefore, the dominant sea level variations of OFES are the most likely to be caused by the atmospheric variations related to the decadal ENSO. It is worth noting that the sea level rise in the 1990s is likely associated with the decadal cooling of SST in the tropical Pacific of more than 0.6°C in the region 9°N–9°S, 100°W–180° from 1992–98 to 1998–2003 (McPhaden and Zhang 2004).

Consistently, the wind stress curl anomalies associated with the decadal ENSO (Fig. 16) are quite similar to those related to OFES-EOF1 (Fig. 12), although the polarity of the anomalies is reversed. For the positive phase of the decadal ENSO, the negative wind stress curl anomalies occur over the central South Pacific and the positive anomalies occur over the northwestern South Pacific and the coast of South America, consistent with the wind stress curl anomalies corresponding to OFES-EOF1. This result supports the concept that atmospheric forcings related to the decadal ENSO cause the sea level variations of OFES-EOF1.

In contrast, the correlation between the low-pass-filtered PC of OFES-EOF1 and the low-pass-filtered AAO index of Marshall (2003) calculated from station SLP data is small, even if we consider time lags. The maximum correlation is found when the PC of OFES-EOF1 leads the AAO index by 13 months, but the correlation is only −0.22. This suggests that OFES-EOF1 is forced primarily by the PSA rather than the AAO, which can be explained by differences of the spatial pattern of the AAO and PSA pattern over the South Pacific. On decadal time scales, the PSA pattern has broad Z500 anomalies (Fig. 14) and large wind stress curl anomalies (Fig. 16) over the central South Pacific, while the AAO pattern has Z500 anomalies (e.g., Thompson et al. 2000; Mo 2000) and large wind stress curl anomalies (not shown) only over the western South Pacific. Hence, the PSA pattern rather than the AAO pattern excites the dominant sea level variations of OFES from 1970 to 2003.

4. Summary and discussion

Sea level variability from 1970 to 2003 in the South Pacific is examined by the EOF analysis using monthly SLAs of OFES along with tide gauge data from 1970 and satellite altimeter data from 1992. The spatial pattern of OFES-EOF1 exhibits broad SLAs in the central and western South Pacific (Fig. 1), consistent with the first EOF mode of the satellite data available after 1992 (Fig. 2). The corresponding PC of OFES-EOF1 indicates roughly stable high, low, and high SLAs, separated by rapid sea level fall in the late 1970s and rapid sea level rise in the late 1990s (Fig. 3). The sea level fall in the late 1970s is also observed from the tide gauge data (Fig. 4), and the sea level rise in the late 1990s is consistent with the satellite data (Fig. 3) and with previous studies (e.g., Cazenave and Nerem 2004). The rapid sea level rise after 1992 in the central and western South Pacific, which attracted much attention because of a possible link to global warming, is not a portion of

a continuous long-term trend, but part of decadal variability.

The sea level variations represented by OFES-EOF1 are related to strength changes of the subtropical gyre from 1970 to 2003 (Fig. 6), consistent with the observed spinup during the 1990s (Roemmich et al. 2007). In addition, the eastward currents around the Tasman Front weaken (strengthen) and the eddy activities decrease (increase) around the northern portion of the Tasman Front in the positive (negative) phase of the OFES-EOF1 (Figs. 7–9). These results indicate that the large-scale gyre, the narrow currents, and the eddy activities all exhibit prominent decadal variability and are associated with the basin-scale sea level fluctuations.

To examine the mechanism of SLAs of OFES-EOF1, we employed a linear long Rossby wave model with a reduced-gravity forced by anomalies of the wind stress curl. This linear model reproduces positive SLAs in the central and western South Pacific in the positive phase of OFES-EOF1 (Figs. 10 and 11). Consistently, broad wind stress curl anomalies over the central South Pacific are strongly correlated at a lead of 1 yr to OFES-EOF1 (Fig. 12). The time integration effect of the wind stress curl anomalies by oceanic Rossby wave amplifies the decadal response (Fig. 13). Hence, the spatial and temporal character of the sea level variations of OFES-EOF1 can be explained by wind-driven long Rossby waves.

The atmospheric fluctuations related to OFES-EOF1 are associated with the decadal variability of ENSO. The large-scale atmospheric changes associated with OFES-EOF1 have broad Z500 anomalies over the central South Pacific (Fig. 14), consistent with the broad wind stress curl anomalies there, and resembles the PSA pattern (Karoly 1989). Although the PSA pattern is the major atmospheric response to ENSO both on interannual and decadal time scales, the oceanic Rossby wave dynamic will make ocean responses more sensitive to the decadal forcings of the PSA pattern. Furthermore, the relation between the decadal ENSO and SLAs in the South Pacific is confirmed by a high correlation between a decadal ENSO index and the PC of OFES-EOF1 (Fig. 15). This high correlation indicates that decadal warming (cooling) in the tropical Pacific accompanies the sea level fall (rise) in the central and western South Pacific. Therefore, it can be concluded that the atmospheric variations related to decadal ENSO, rather than the previously argued AAO, cause the SLAs of OFES-EOF1.

The result that the overall SLAs of OFES-EOF1 are explained by baroclinic long Rossby waves can be useful to understand fluctuations of marine ecosystem in the South Pacific, especially in the Tasman Sea, the location of the largest noncoastal surface chlorophyll-a concentrations in the South Pacific (Tilburg et al. 2002). Wilson and Coles (2004) showed that surface chlorophyll-a concentrations are positively related to the thermocline depth in the Tasman Sea. Because sea level rise caused by a first baroclinic Rossby wave is accompanied by a deepening of the thermocline, high SLAs predicted by the linear model are expected to accompany elevated concentrations of the chlorophyll-a. Because sea level variability in the Tasman Sea is mainly caused by long Rossby waves from east of New Zealand (Fig. 11), atmospheric variations over the central South Pacific associated with decadal ENSO are expected to influence the marine ecosystems in the Tasman Sea.

The conclusion that the decadal sea level changes are due to the decadal ENSO has important implications on future projections of sea level in the South Pacific associated with global warming. Because future projections suggest a relation between trends of global warming and AAO (e.g., Fyfe et al. 1999; Cai et al. 2003; Meehl et al. 2007), numerical studies of an ocean model focused on the atmosphere changes related to the AAO for a response of the South Pacific Ocean circulation to global warming (e.g., Oke and England 2004; Cai et al. 2005). However, global warming is expected to influence ENSO variability (e.g., Knutson and Manabe 1998; Yamaguchi and Noda 2006; Meehl et al. 2007), and a majority of different coupled ocean–atmosphere general circulation models showed an El Niño–like response under global warming (Yamaguchi and Noda 2006). If this is the case, our results suggest that sea level will fall in the central and western South Pacific, opposite to the recent sea level rise. However, because it is expected that both the AAO and ENSO changes influence atmospheric variations over the South Pacific, it is necessary to determine which change dominates over the South Pacific. Yamaguchi and Noda (2006) mentioned that the relative importance of an El Niño–like trend and an Arctic Oscillation–like trend for atmospheric variations over the North Pacific under global warming is different in the current models. Hence, to understand future sea level and associated ocean circulation changes in the South Pacific, it is important to understand the relative importance of the AAO and ENSO changes for the future atmospheric changes over the South Pacific.

Acknowledgments. We thank S.-P. Xie and B. Qiu for fruitful discussions and comments, and D. Roemmich for preprints. We also appreciate two anonymous reviewers for comments that helped to improve the manuscript. This study was supported by grant-in-aid for scientific research (kaken-hi, to SM) by the 21st

Century Center of Excellence Program on "Neo-Science of Natural History" led by H. Okada from the Ministry of Education, Culture, Sports, Science and Technology, Japan, and by the Office of Science (BER), U.S. Department of Energy Grants DE-FG02-04ER63862 and DE-FG02-07ER64469. YS is a research fellow of the Japan Society for the Promotion of Science. The OFES simulation was conducted on the Earth Simulator under support of JAMSTEC.

REFERENCES

Andrews, J. C., M. W. Lawrence, and C. S. Nilsson, 1980: Observations of the Tasman Front. *J. Phys. Oceanogr.,* **10,** 1854–1869.

Barnier, B., 1988: A numerical study on the influence of the mid-Atlantic ridge on nonlinear first-mode baroclinic Rossby waves generated by seasonal winds. *J. Phys. Oceanogr.,* **18,** 417–433.

Bowen, M. M., J. L. Wilkin, and W. J. Emery, 2005: Variability and forcing of the East Austraian Current. *J. Geophys. Res.,* **110,** C03019, doi:10.1029/2004JC002533.

——, P. J. H. Sutton, and D. Roemmich, 2006: Wind-driven and steric fluctuations of sea surface height in the southwest Pacific. *Geophys. Res. Lett.,* **33,** L14617, doi:10.1029/2006GL026160.

Boyer, T. P., S. Levitus, J. I. Antonov, M. E. Conkright, T. O'Brien, and C. Stephen, 1998a: *Salinity of the Atlantic Ocean*. Vol. 4, *World Ocean Atlas 1998,* NOAA Atlas NESDIS 30, 166 pp.

——, ——, ——, ——, ——, and ——, 1998b: *Salinity of the Pacific Ocean*. Vol. 5, *World Ocean Atlas 1998,* NOAA Atlas NESDIS 31, 166 pp.

——, ——, ——, ——, ——, ——, and B. Trotsenko, 1998c: *Salinity of the Indian Ocean*. Vol. 6, *World Ocean Atlas 1998,* NOAA Atlas NESDIS 32, 166 pp.

Cai, W., P. H. Whetton, and D. J. Karoly, 2003: The response of the Antarctic Oscillation to increasing and stabilized atmospheric CO_2. *J. Climate,* **16,** 1525–1538.

——, G. Shi, T. Cowan, D. Bi, and J. Ribbe, 2005: The response of the Southern Annular Mode, the East Australian Current, and the southern mid-latitude ocean circulation to global warming. *Geophys. Res. Lett.,* **32,** L23706, doi:10.1029/2005GL024701.

Cazenave, A., and R. S. Nerem, 2004: Present-day sea level change: Observations and causes. *Rev. Geophys.,* **42,** RG3001, doi:10.1029/2003RG000139.

Chavez, F. P., J. Ryan, S. E. Lluch-Cota, and C. M. Niquen, 2003: From anchovies to sardines and back: Multidecadal change in the Pacific Ocean. *Science,* **299,** 217–221.

Chelton, D. B., R. A. de Szoeke, M. G. Schlax, K. E. Naggar, and N. Siwertz, 1998: Geographical variability of the first baroclinic Rossby radius of deformation. *J. Phys. Oceanogr.,* **28,** 433–460.

Church, J. A., J. M. Gregory, P. Huybrechts, M. Kuhn, K. Lambeck, M. T. Nhuan, D. Qin, and P. L. Woodworth, 2001: Changes in sea level. *Climate Change 2001: The Scientific Basis,* J. T. Houghton et al., Eds., Cambridge University Press, 639–694.

Ducet, N., P. Y. Le Traon, and G. Reverdin, 2000: Global high-resolution mapping of ocean circulation from TOPEX/Poseidon and ERS-1 and -2. *J. Geophys. Res.,* **105,** 19 477–19 498.

Folland, C. K., D. E. Parker, A. Colman, and R. Washington, 1999: Large scale modes of ocean surface temperature since the late nineteenth century. *Beyond El Niño: Decadal and Interdecadal Climate Variability,* A. Navarra, Ed., Springer-Verlag, 73–102.

Fu, L.-L., and B. Qiu, 2002: Low-frequency variability of the North Pacific Ocean: The roles of boundary- and wind-driven baroclinic Rossby waves. *J. Geophys. Res.,* **107,** 3220, doi:10.1029/2001JC001131.

Fyfe, J. C., G. J. Boer, and G. M. Flato, 1999: The Arctic and Antarctic Oscillations and their projected changes under global warming. *Geophys. Res. Lett.,* **26,** 1601–1604.

Garreaud, R. D., and D. S. Battisti, 1999: Interannual (ENSO) and interdecadal (ENSO-like) variability in the Southern Hemisphere tropospheric circulation. *J. Climate,* **12,** 2113–2123.

Godfrey, J. S., 1989: A Sverdrup model of the depth-integrated flow for the world ocean allowing for island circulations. *Geophys. Astrophys. Fluid Dyn.,* **45,** 89–112.

Goring, D. G., and R. G. Bell, 1999: El Niño and decadal effects on sea level variability in northern New Zealand: A wavelet analysis. *N. Z. J. Mar. Freshwater Res.,* **33,** 587–598.

Häkkinen, S., and P. B. Rhines, 2004: Decline of subpolar North Atlantic circulation during the 1990s. *Science,* **304,** 555–559.

Hannah, J., 2004: An updated analysis of long-term sea level change in New Zealand. *Geophys. Res. Lett.,* **31,** L03307, doi:10.1029/2003GL019166.

Hines, K. M., D. H. Bromwich, and G. J. Marshall, 2000: Artificial surface pressure trends in the NCEP–NCAR reanalysis over the Southern Ocean and Antarctica. *J. Climate,* **13,** 3940–3952.

Isoguchi, O., and H. Kawamura, 2006: Seasonal to interannual variations of the western boundary current of the subarctic North Pacific by a combination of the altimeter and tide gauge sea level. *J. Geophys. Res.,* **111,** C04013, doi:10.1029/2005JC003080.

Kalnay, E., and Coauthors, 1996: The NCEP/NCAR 40-Year Reanalysis Project. *Bull. Amer. Meteor. Soc.,* **77,** 437–471.

Karoly, D. J., 1989: Southern Hemisphere circulation features associated with El Niño–Southern Oscillation events. *J. Climate,* **2,** 1239–1252.

Knutson, T. R., and S. Manabe, 1998: Model assessment of decadal variability and trends in the tropical Pacific ocean. *J. Climate,* **11,** 2273–2296.

Liu, Z., L. Wu, and H. Hurlburt, 1999: Rossby wave–coastal Kelvin wave interaction in the extratropics. Part II: Formation of island circulation. *J. Phys. Oceanogr.,* **29,** 2405–2418.

Maharaj, A. M., P. Cipolloni, and N. J. Holbrook, 2005: Observed variability of the South Pacific westward sea level anomaly signal in the presence of bottom topography. *Geophys. Res. Lett.,* **32,** L04611, doi:10.1029/2004GL020966.

Mantua, N. J., S. R. Hare, Y. Zhang, J. M. Wallace, and R. C. Francis, 1997: A Pacific interdecadal climate oscillation with impacts on salmon production. *Bull. Amer. Meteor. Soc.,* **76,** 1069–1079.

Marshall, G. J., 2003: Trends in the Southern Annular Mode from observations and reanalyses. *J. Climate,* **16,** 4134–4143.

——, and S. A. Harangozo, 2000: An appraisal of NCEP/NCAR reanalysis MSLP data variability for climate studies in the South Pacific. *Geophys. Res. Lett.,* **27,** 3057–3060.

Masumoto, Y., and Coauthors, 2004: A fifty-year eddy-resolving

simulation of the world ocean—Preliminary outcomes of OFES (OGCM for the Earth Simulator). *J. Earth Simulator,* **1,** 35–56.

Mata, M. M., S. E. Wijiffels, J. A. Church, and M. Tomczak, 2006: Eddy shedding and energy conversions in the East Australian Current. *J. Geophys. Res.,* **111,** C09034, doi:10.1029/2006JC003592.

McCalpin, J. D., 1995: Rossby wave generation by poleward propagating Kelvin waves: The midlatitude quasigeostrophic approximation. *J. Phys. Oceanogr.,* **25,** 1415–1425.

McPhaden, M. J., and D. Zhang, 2004: Pacific Ocean circulation rebounds. *Geophys. Res. Lett.,* **31,** L18301, doi:10.1029/2004GL020727.

Meehl, G. A., and Coauthors, 2007: Global climate projections. *Climate Change 2007: The Physical Science Basis,* S. Solomon et al., Eds., Cambridge University Press, 747–845.

Minobe, S., 1997: A 50–70 year climatic oscillation over the North Pacific and North America. *Geophys. Res. Lett.,* **24,** 683–686.

——, 2002: Interannual to interdecadal changes in the Bering Sea and concurrent 1998/99 changes over the North Pacific. *Prog. Oceanogr.,* **55,** 45–64.

Mo, K. C., 2000: Relationship between low-frequency variability in the Southern Hemisphere and sea surface temperature anomalies. *J. Climate,* **13,** 3599–3610.

Nonaka, M., H. Nakamura, Y. Tanimoto, T. Kagimoto, and H. Sasaki, 2006: Decadal variability in the Kuroshio–Oyashio Extension simulated in an eddy-resolving OGCM. *J. Climate,* **19,** 1970–1989.

Oke, P. R., and M. H. England, 2004: Oceanic response to changes in the latitude of the Southern Hemisphere subpolar westerly winds. *J. Climate,* **17,** 1040–1054.

Pacanowski, R. C., and S. M. Griffies, 1999: The MOM3 manual. NOAA/GFDL Ocean Group Tech. Rep. 4, 680 pp.

Pedlosky, J., 1987: *Geophysical Fluid Dynamics*. Springer-Verlag, 710 pp.

——, L. J. Pratt, M. A. Spall, and K. R. Helfrich, 1997: Circulation around islands and ridges. *J. Mar. Res.,* **55,** 1199–1251.

Power, S., T. Casey, C. Folland, A. Colman, and V. Mehta, 1999: Inter-decadal modulation of the impact of ENSO on Australia. *Climate Dyn.,* **15,** 319–324.

Qiu, B., 2003: Kuroshio Extension variability and forcing of the Pacific decadal oscillations: Responses and potential feedback. *J. Phys. Oceanogr.,* **33,** 2465–2482.

——, and S. Chen, 2004: Seasonal modulations in the eddy field of the South Pacific Ocean. *J. Phys. Oceanogr.,* **34,** 1515–1527.

——, and ——, 2006: Decadal variability in the large-scale sea surface height field of the South Pacific Ocean: Observations and causes. *J. Phys. Oceanogr.,* **36,** 1751–1762.

Rayner, N. A., D. E. Parker, E. B. Horton, C. K. Folland, L. V. Alexander, D. P. Rowell, E. C. Kent, and A. Kaplan, 2003: Global analyses of sea surface temperature, sea ice, and night marine air temperature since the late nineteenth century. *J. Geophys. Res.,* **108,** 4407, doi:10.1029/2002JD002670.

Reid, J., 1986: On the total geostrophic circulation of the South Pacific Ocean: Flow patterns, tracers, and transports. *Prog. Oceanogr.,* **39,** 263–352.

Ridgway, K. R., and J. R. Dunn, 2003: Mesoscale structure of the mean East Australian Current system and its relationship with topography. *Prog. Oceanogr.,* **56,** 189–222.

Roemmich, D., J. Gilson, R. Davis, P. Sutton, S. Wijffels, and S. Riser, 2007: Decadal spinup of the South Pacific subtropical gyre. *J. Phys. Oceanogr.,* **37,** 162–173.

Rosati, A., and K. Miyakoda, 1988: A general circulation model for upper ocean circulation. *J. Phys. Oceanogr.,* **18,** 1601–1626.

Sasaki, H., and Coauthors, 2004: A series of eddy-resolving ocean simulations in the world ocean: OFES (OGCM for the Earth Simulator) project. *Proc. Oceans'04/MTS/IEEE/Techno-Ocean'04,* Vol. 3, 1535–1541.

——, M. Nonaka, Y. Masumoto, Y. Sasai, H. Uehara, and H. Sakuma, 2007: An eddy-resolving hindcast simulation of the quasi-global ocean from 1950 to 2003 on the Earth Simulator. *High Resolution Numerical Modeling of the Atmosphere and Ocean,* W. Ohfuchi and K. Hamilton, Eds., Springer, 157–186.

Schneider, N., A. J. Miller, and D. W. Pierce, 2002: Anatomy of North Pacific decadal variability. *J. Climate,* **15,** 586–605.

Sutton, P. J., M. Bowen, and D. Roemmich, 2005: Decadal temperature changes in the Tasman Sea. *N. Z. J. Mar. Freshwater Res.,* **39,** 1321–1329.

Taguchi, B., S.-P. Xie, N. Schneider, M. Nonaka, H. Sasaki, and Y. Sasai, 2007: Decadal variability of the Kuroshio Extension: Observations and an eddy-resolving model hindcast. *J. Climate,* **20,** 2357–2377.

Thompson, D. W. J., J. M. Wallace, and G. C. Hegerl, 2000: Annular modes in the extratropical circulation. Part II: Trends. *J. Climate,* **13,** 1018–1036.

Tilburg, C. E., H. E. Hurlburt, J. J. O'Brien, and J. F. Shriver, 2001: The dynamics of the East Australian Current system: The Tasman Front, the East Auckland Current, and the East Cape Current. *J. Phys. Oceanogr.,* **31,** 2917–2943.

——, B. Subrahmanyam, and J. J. O'Brien, 2002: Ocean color variability in the Tasman Sea. *Geophys. Res. Lett.,* **29,** 1487, doi:10.1029/2001GL014071.

Vega, A., Y. du-Penhoat, B. Dewitte, and O. Pizarro, 2003: Equatorial forcing of interannual Rossby waves in the eastern South Pacific. *Geophys. Res. Lett.,* **30,** 1197, doi:10.1029/2002GL015886.

Wilson, C., and V. J. Coles, 2004: Global climatological relationships between satellite biological and physical observations and upper ocean properties. *J. Geophys. Res.,* **110,** C10001, doi:10.1029/2004JC002724.

Woodworth, P. L., and R. Player, 2003: The permanent service for mean sea level: An update to the 21th century. *J. Coastal Res.,* **19,** 287–295.

Yamaguchi, K., and A. Noda, 2006: Global warming patterns over the North Pacific: ENSO versus AO. *J. Meteor. Soc. Japan,* **84,** 221–241.

Zhang, Y., J. M. Wallace, and D. S. Battisti, 1997: ENSO-like interdecadal variability: 1900–93. *J. Climate,* **10,** 1004–1020.